Single-cycle THz-field electro-optical sampling with single-photon detectors

Taylor Shields[1,*], Adetunmise C. Dada[2], Lennart Hirsch[1], Seungjin Yoon[1], Jonathan M. R. Weaver[1], Daniele Faccio[2], Lucia Caspani[3], Marco Peccianti[4], Matteo Clerici[1,]**

[1]James Watt School of Engineering, University of Glasgow, Glasgow G12 8QQ, United Kingdom
[2]School of Physics and Astronomy, University of Glasgow, Glasgow G12 8QQ, United Kingdom
[3]Institute of Photonics, Department of Physics, University of Strathclyde, Glasgow G1 1RD, United Kingdom
[4]Emergent Photonics Research Centre and Dept. of Physics, Loughborough University, Loughborough, LE11 3TU, UK
[*]t.shields.1@research.gla.ac.uk, **matteo.clerici@glasgow.ac.uk

ABSTRACT

Terahertz time-domain spectroscopy (THz-TDS) using electro-optic sampling and ultrashort pulsed probes is a well-established technique for directly measuring the electric field of THz radiation. Traditionally, a balanced detection scheme relies on measuring an optical phase shift brought by THz-induced birefringence radiation using photodiodes, where sensitivity is limited by the shot-noise of the optical-sampling probe. Improvement to the sensitivity of such an approach could be achieved by applying quantum metrology, such as using NOON states for Heisenberg-limited phase estimation. We report on the first step in that direction, demonstrating that THz electric fields can be measured with single-photon detectors using a squeezed vacuum as the optical probe. Our approach achieves THz electro-optical sampling using phase-locked single-photon detectors at the shot-noise limit and thus paves the way toward quantum-enhanced THz sensing.

Introduction

Terahertz radiation is traditionally defined as the range of the electromagnetic spectrum between the microwave and infrared spectral regions and in recent years has garnered significant interest in fields such as imaging, medicine, communications etc[1-5]. A wide range of applications of THz radiation relies on THz time-domain spectroscopy (THz-TDS), a technique able to measure the electric field (phase and amplitude) of a THz pulse. This uses ultrafast laser pulses to generate and subsequently measure the THz field in the time domain exploiting nonlinear optical processes. A well-established THz-TDS system approach is based on electro-optic sampling, a form of time-resolved polarimetry that utilizes the Pockels Effect in second-order nonlinear crystals to induce a phase shift proportional to the THz field strength[6-9]. This way, the THz pulse can be reconstructed in the time domain if the probe pulse is shorter than the THz electric field oscillation period. Currently, the sensitivity of THz-TDS is limited by the shot-noise of the optical probes used for sampling the THz field. Recent efforts to enhance performance have targeted the detection strategy[10] while, very recently, proposals to enhance the THz sensitivity using nonclassical radiation have been proposed[11]. NOON or Fock ultrashort probe states may improve polarimetric measurements[12,13] and could be applied to the THz-TDS. In this work, we implemented electro-optical sampling with ultrashort squeezed vacuum radiation generated by parametric down-conversion of a 100 fs duration optical pulse at 780 nm in a periodically-poled lithium niobate crystal. To this end, we developed a scheme to perform a lock-in style polarimetry with single-photon detectors, achieving shot-noise limited detection and paving the way for the use of nonclassical probes in THz

electro-optical sampling aiming toward quantum-enhanced time-domain spectroscopy. We used squeezed vacuum, i.e., the radiation generated by spontaneous parametric down-conversion in a second-order nonlinear medium, rather than a weak coherent probe pulse, as the former is a widely employed resource underpinning quantum-enhanced metrology.

Standard THz-TDS measurement

As a first step, we generated a broadband (single-cycle) THz electric field and we measured it in a standard THz-TDS set-up, as described below. The single-cycle THz radiation is generated by a photoconductive antenna (Tera-SED, Laser Quantum) photo-excited with a train of ultrashort light pulses delivered by a mode-locked laser (Coherent Discovery) with an average power of 600 mW, pulse duration of 100 fs, 80 MHz repetition rate, and central wavelength of 780 nm. The THz antenna consists of a planar 3×3 mm^2 GaAs substrate with an interdigitated metal-semiconductor-metal electrode structure, which is modulated by an externally applied bias field. The photoconductive antenna (PCA) employed delivers a single-cycle THz field with a peak emission frequency of 1.5 THz. The excitation condition was optimized by recording the THz power with a pyroelectric detector (THZ5I-BL-BNC-D0, Gentec EO) aided by a low noise current mode amplifier and using a 5 Hz chopping frequency[14,15]. The THz electric field trace is then measured using a conventional THz-TDS setup. In our setting, the birefringence of an AR-coated (1560 nm) GaAs <110> crystal is modulated by the THz electric field and probed by polarimetry performed with a short optical pulse overlapped to different temporal sections of the THz field[16]. The residual pump field incident on the PCA is removed with a paper filter before reaching the detection crystal. A 200 fs probe pulse used the optical sampling is delivered by an Optical Parametric Oscillator (OPO, Levante IR, Coherent) tuned at 1560 nm, at the same wavelengths of the squeezed vacuum source employed for the single-photon-level measurement. The relative delay between the probe and the THz pulses is controlled by a delay stage (Newport, M-VP-25XL). The phase delay induced by the THz field on the probe pulse is analyzed by means of a standard polarimetric arrangement comprised of a quarter-wave plate ($\lambda/4$, Newport 10RP04-40) followed by a Wollaston prism (Thorlabs WPA10) and a balanced detector (Thorlabs, PDB210C/M). The THz and the probe field were cross-polarized and the orientation of the GaAs was optimized to maximize the electro-optical modulation[17]. The quarter-waveplate is oriented in such a way that no differential signal is produced by a probe injected into the setup in absence of the THz field. The balanced detector amplified signal is measured and digitalized by a lock-in amplifier (Stanford Research, SR8300), synchronized to the 10 kHz signal employed to modulate (on-off) the 30 V bias voltage applied to the photoconductive antenna. Using high lock-in frequencies allows for reducing the impact of the $1/f$ noise [18-20]. In Fig. 1A we show an example of a THz trace acquired after purging our setup with pure nitrogen to reduce atmospheric water absorption. In Fig. 1B we show the spectrum obtained by Fourier transform of the time domain signal in Fig. 1A (red curve), and the spectrum obtained for a similar scan in a non-purged condition for comparison (blue curve), where the strong absorption features of atmospheric water are clearly evident[21,22]. The amplitude $E_{THz}(t)$ of the measured THz electric field trace $E_{tr}(t)$ was calibrated according to:

$$E_{THz}(t) = \frac{E_{tr}(t)}{max(|\mathcal{E}_{tr}(t)|)} \sqrt{\frac{2U\eta_0}{\int G(x,y)\,dx\,dy \int \frac{|\mathcal{E}_{tr}(t)|^2}{max(|\mathcal{E}_{tr}(t)|^2)}\,dt}}$$

where $\mathcal{E}(t)$ is the complex electric field trace, such that $E_{tr}(t) = Re[\mathcal{E}_{tr}(t)]$, $U \simeq 1.25$ fJ is the THz pulse energy measured with the pyroelectric detector, $G(x,y) = \exp\left(-x^2/{\sigma_x}^2 - y^2/{\sigma_y}^2\right)$ is the THz beam profile determined by knife-edge

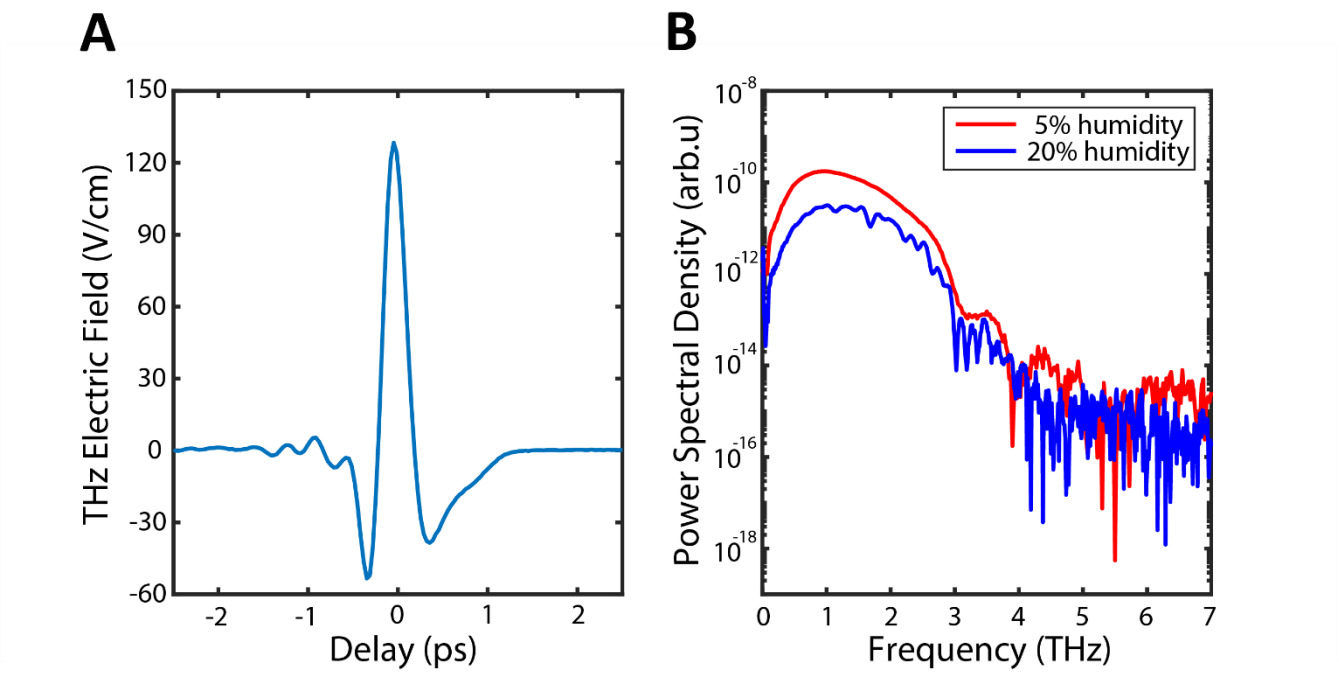

Figure 1 (A) THz time-domain spectroscopy using electro-optic sampling to characterize the THz field trace and spectrum using a classical balanced detection scheme. (B) Power spectrum corresponding to the measurement in A (red curve) and in an un-purged setup (blue curve).

measurements with $\sigma_x = \sigma_y = 200 \pm 10$ µm, and η_0 is the vacuum impedance[23]. According to this calibration, the THz field amplitude reached a peak value in air of $\simeq 130$ V/cm as shown in Figure 1A.

A crucial step required to perform the THz measurement with single photon detectors is to assess the detection system sensitivity and the magnitude of phase shift our generated field impart on a probe field. To this end, we have estimated the maximum phase shift $\Delta\Phi \simeq \frac{\Delta I_p}{I_p}$ (relative difference in the probe signal intensity between the two photodiodes) that the THz field generated in our experiment will be able to impart to a probe field inside the detection crystal according to

$$\Delta\Phi = \left|\frac{E_{THz} r_{41} n^3 \omega L}{c}\right|,$$

where r_{41}, n and L are the detection crystal electro-optical coefficient, refractive index and thickness[17,24]. Using the recorded THz field amplitude and considering $n = 3.38$ and $L = 300$ µm we estimate a maximum phase shift of $\Delta\Phi \simeq 2.4 \times 10^{-4}\pi$. Estimation of the maximum phase shift our peak field induces allowed us to estimate the integration time required in order to observe the phase change due to the THz electric field with single-photon detectors.

Generation of squeezed vacuum and measurement calibration

Once the THz radiation properties were characterized using a standard THz-TDS setup using a coherent probe and proportional detectors, we set up the squeezed vacuum source to be used as alternative probe pulse. The squeezed vacuum, with a wavelength centered at 1560 nm, was generated by Type 0 parametric down-conversion (PDC) of the 780 nm pump laser in a 0.5 mm long periodically poled Magnesium-doped lithium niobate crystal (MgO-PPLN, Covesion, MSHG1550-0.5, 19.70 µm). Off-axis parabolic mirrors of equivalent focal length 50 mm were used to focus the pump beam to 13 µm into the crystal and to collect and collimated the generated radiation. We first characterized the source in the high photon flux regime using

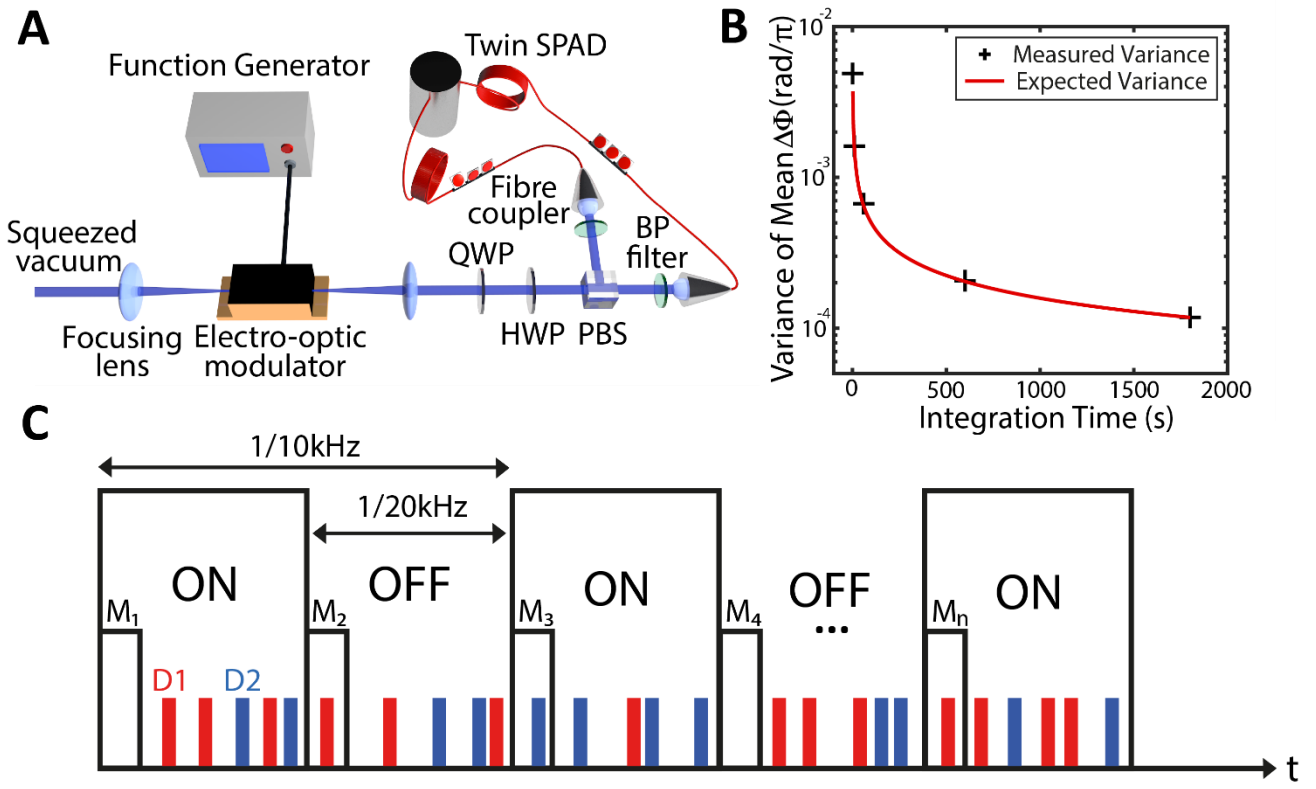

Figure 2. Calibration setup with EOM and experimental lock-in balanced detection scheme using two single photon detectors. (A) Experimental scheme for calibration of detection using electro-optic modulation. (B) Measured variance of the detection method using EOM with single photon counts indicating the measurement is shot-noise limited. (C) Using ps-time tagging resolution of the photon counting software, a difference measurement was performed between counts of detectors D1 (red) and D2 (blue) using markers M inserted every 20 kHz to synchronize timing with the antenna modulation.

an amplified InGaAs photodiode (Thorlabs PDA10DT) varying the crystal temperature to maximize the flux within a 12 nm spectral region centered at 1560 nm (Thorlabs FBH1550-12). We then routed the squeezed vacuum radiation into the balanced detection setup employed for the characterization of the THz-induced phase shift. Differently from before, however, the collimated output of the polarimetric setup is coupled into optical fiber using reflective collimator couplers (Thorlabs RC04FC-P01). A lens telescope (f_1 = -75 mm, f_2 = +150 mm) was also inserted into the beam path to optimize the coupling. The radiation was then measured with InGaAs-based Single-Photon Avalanche Photodiodes (ID Quantique, ID230). These detectors can record single photons at a maximum rate of 1MHz and with 25% quantum efficiency. The arrival time of single photons was digitalized with time-tagging electronics (PicoQuant HydraHarp).

To calibrate our single-photon-detector-based polarimetry setup and to assess its phase sensitivity, we used an electro-optical modulator (Thorlabs, EO-AM-NR-C3), as shown in Fig. 2A, configured to change the polarization of the injected radiation. The half-wave voltage (V_π) at the operating wavelength was 539 V, and the EOM was driven by a high voltage amplifier (max 200 V, Thorlabs HVA200) fed with a modulated signal. In an ideal case, the phase shift induced by the EOM will result in an unbalance of the signal on one photon counter with respect to the other, such that $\Delta N = (\langle N_1 \rangle + \langle N_2 \rangle)\Delta\Phi$, where $\langle N_1 \rangle$ and $\langle N_2 \rangle$ are the average counts of 200 kHz on the two detectors. In a shot-noise limited measurement, the minimum detectable phase shift will then be $\sigma(\Delta\Phi) \approx (\langle N_1 \rangle + \langle N_2 \rangle)^{-\frac{1}{2}}$ which is how the expected variance is estimated in Fig. 2B[12]. However, to achieve shot-noise limited detection, other sources of technical noise must be removed. To this end, we have implemented a

digital analogue of lock-in detection shown in Fig. 2C, performed by modulating the EOM using a square wave with a 10 kHz period and introducing markers in the time-tagged data at double such frequency. We note that the modulation frequency is the same used to drive the antenna for the THz measurement described above. The differential signal at the modulation period n is then calculated as

$$\Delta\Phi_n = \frac{\Delta N_{n,\mathrm{on}}}{\sum N_1 + \sum N_2} - \frac{\Delta \mathrm{N}_{\mathrm{n,off}}}{\sum N_1 + \sum N_2},$$

where on and off refer to the sections of the time-tagged data where the modulation was active or inactive, respectively. We numerically estimated the variance of the measured phase shift for increasing integration time at constant measured photon rate. The results are shown Fig. 2B (blue crosses) and compared to the expected shot-noise limited performance assuming Poissonian statistics in the input field[25,26].

THz field measurement with single-photon detectors

From the estimated THz peak field measured with the classical THz-TDS setup ($\simeq 130\ \mathrm{V/cm}$, corresponding to a phase shift of $\Delta\Phi \simeq 2.4 \times 10^{-4}\pi$), and the experimentally confirmed shot-noise limited detection sensitivity of our single-photon level polarimetric scheme, we expected that the THz-induced phase shift would become visible (at the peak) after 10 minutes of acquisition determined using the estimated phase shift and a 800 kHz photon rate. We, therefore, substituted the EOM with the GaAs detection crystal excited with the THz radiation, purged the generation and detection area with nitrogen, and recorded the data as described above. A complete sketch of the experimental setup is shown in Fig. 3A. Figure 3B shows the measured phase shift induced by the THz radiation on the infrared squeezed vacuum probe pulse as a function of their relative delay (blue squares) compared against the THz trace measured with the classical THz-TDS obtained via electro-optic sampling (red curve, normalized). This measurement demonstrates that it is possible to perform THz-TDS with a probe pulse at the single-photon level (with an estimated average of 0.01x photons per pulse) and provides the first proof of an ultrafast phase modulation applied within a picosecond window on squeezed vacuum radiation.

The observed phase shift of $\Delta\Phi \simeq 1.35 \times 10^{-4}\pi$ is lower than the value expected from the one measured with the intense classical probe ($2.4 \times 10^{-4}\pi$). We attributed this small difference to the shorter duration of the squeezed vacuum respect to the coherent pulse and residual spatial overlap issues. The THz electric field trace measured with squeezed vacuum is also shorter than what was recorded with a coherent probe. The difference can be attributed to the shortened duration of the squeezed vacuum (<100 fs) with respect to the coherent pulse (~200 fs). The shot-noise limited nature of the measurement can be observed in Figure 3C where the phase noise at the THz peak temporal coordinate is measured (blue crosses) and plotted against the expected values (red curve).

Conclusions

Using a lock-in style phase detection method, we have demonstrated time-resolved detection of THz single-cycle pulses employing a squeezed vacuum source and single-photon detectors. The acquisition setup is shot-noise limited and allowed the observation of a weak THz single-cycle pulse with peak amplitude of $\simeq 130\ \mathrm{V/cm}$ with a signal-to-noise ratio of 5 for an acquisition time of 105 minutes. While no quantum enhancement in the THz detection can be proved at this stage, our work lays the basis to investigate further the possibility to apply quantum-metrology strategies to enhance the detection sensitivity of THz fields, employing as a probe light for the THz-TDS scheme non-classical resources such as NOON states or single-

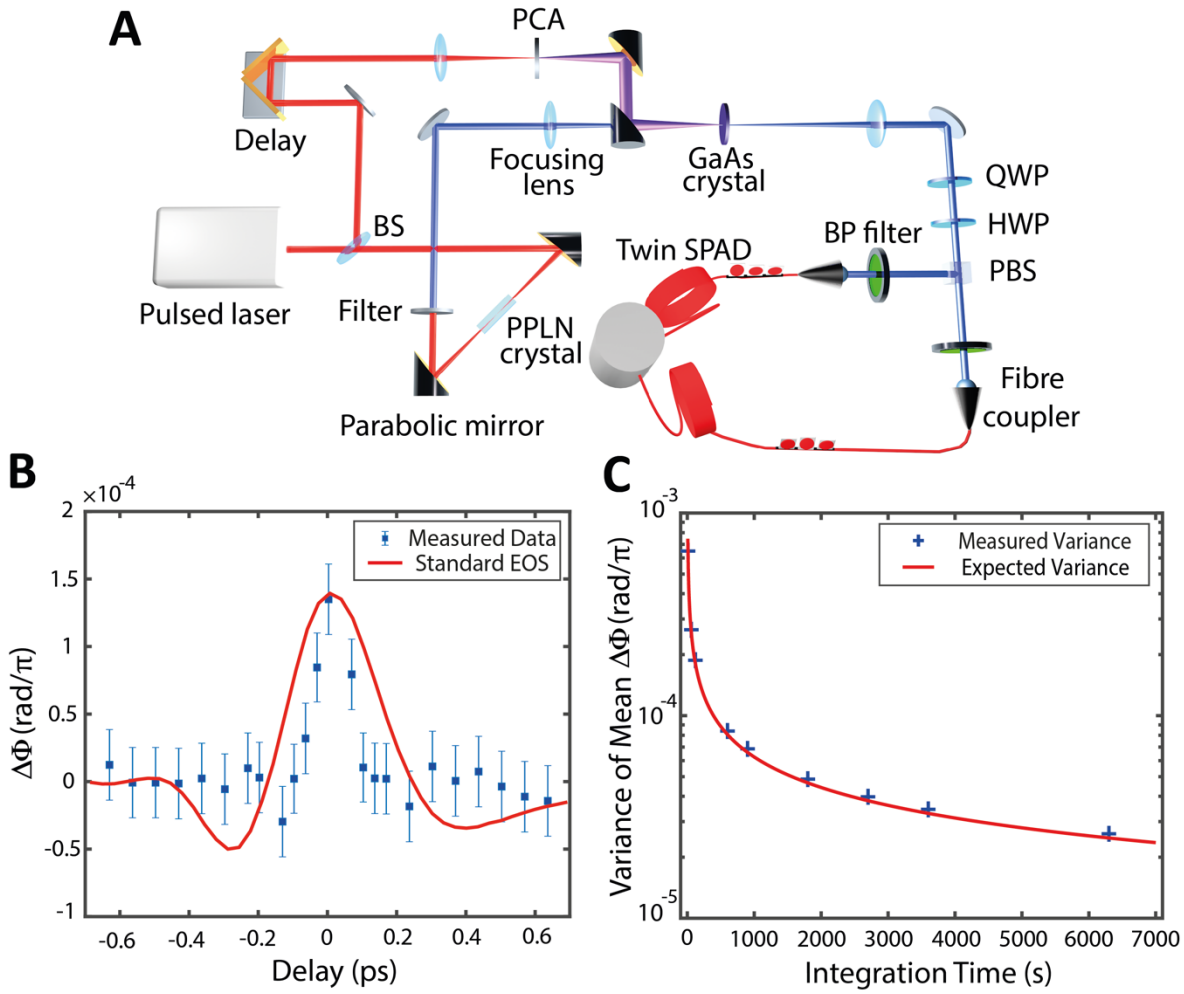

Figure 3. Terahertz detection using single photons. (A) Experimental scheme for measuring THz field using squeezed vacuum. The THz field generated from a photoconductive antenna (PCA) is overlapped to the squeezed vacuum pulse into a GaAs electro-optical crystal. The phase shift introduced by the THz pulse on the squeezed vacuum probe is measured by a balanced detection using single photon detectors. (B) Measured phase shift ($\Delta\Phi$) induced by THz field (blue squares) overlapped with the phase shift from standard electro-optic sampling (EOS) scaled to the measured value (red line). The integration time for each data point was 105 mins. (C) Measured variance of the detection method indicating the final measurement is shot-noise limited so THz field is not adding noise.

photons. Furthermore, we have shown that sub-picosecond single-cycle THz pulses can be employed to impart a phase shift to independently detected photons, albeit limited in our case to < 0.5 mrad. As large THz peak fields can be achieved enabling full-wave phase shifts, we foresee a potential application of the scheme demonstrated here to ultrafast encoding of phase information[27] and polarization demultiplexing in single-photon applications.

References

1. Johnston, M. B. *et al.* Simulation of terahertz generation at semiconductor surfaces. *Phys. Rev. B.* **65**, 165301, DOI: 10.1103/PhysRevB.65.165301 (2002)
2. Luo, L. *et al.* Broadband terahertz generation from metamaterials. *Nat. Commun.* **5**, 3055, DOI: 10.1038/ncomms4055 (2014)

3. Shen, Y. C. *et al*. Detection and identification of explosives using terahertz pulsed spectroscopic imaging. *Appl. Phys. Lett*. **86**, 241116, DOI: 10.1063/1.1946192 (2005)
4. Park, S. J. *et al.* Sensing viruses using terahertz nano-gap metamaterials. *Biomed. Opt. Express* **8**, 3551, DOI: 10.1364/BOE.8.003551 (2017)
5. Kampfrath, T., Tanaka, K. & Nelson, K. A. Resonant and nonresonant control over matter and light by intense terahertz transients. *Nat.Photonics*, **7**, 680, DOI: 10.1038/NPHOTON.2013.184 (2013)
6. Auston, D. H. *et al*. Picosecond optoelectronic detection, sampling, and correlation measurements in amorphous semiconductors. *Appl. Phys. Lett.* **37** (4), 371–373, DOI: 10.1063/1.91947 (1980)
7. Valdmanis, J. A., Mourou, G. A. & Gabel, C. W. Subpicosecond electrical sampling. *IEEE J. Quantum Electron.* **19** (4), 664–667, DOI: 10.1109/JQE.1983.1071915 (1983)
8. Auston, D. H. & Nuss, M. C. Electrooptical generation and detection of femtosecond electrical transients. *IEEE J. Quantum Electron*. **24**(2), 184–197, DOI: 10.1109/3.114 (1988)
9. Xu, L., Zhang, X.-C. & Auston, D. H. Terahertz beam generation by femtosecond optical pulses in electro-optic materials, *Appl. Phys. Lett.* **61** (15), 1784–1786, DOI: 10.1063/1.108426 (1992)
10. Porer, M., Ménard, J-M. & Huber, R. Shot noise reduced terahertz detection via spectrally postfiltered electro-optic sampling. *Opt. Lett.* **39**, 8, DOI: 10.1364/OL.39.002435 (2014)
11. Virally, S., Cusson, P. & Seletskiy, D. V. Enhanced Electro-Optic Sampling with Quantum Probes. *Phys. Rev. Lett.* **127**, 270504, DOI: 10.1103/PhysRevLett.127.270504 (2021)
12. Yoon, S., Lee, J., Rockstuhl, C., Lee, C., Lee, K. Experimental quantum polarimetry using heralded single photons. *Metrologia.* **57**, 045008, DOI: 10.1088/1681-7575/ab8801 (2020)
13. Taylor, M. Quantum Microscopy of Biological Systems. Springer (2015)
14. Dreyhaupt, A. *et al.* Optimum excitation conditions for the generation of high-electric-field terahertz radiation from an oscillator-driven photoconductive device. *Opt. Lett.* **31**, 1546, DOI: 10.1364/OL.31.001546 (2006)
15. Xu, J. Z. & Zhang, X.-C. Optical rectification in an area with a diameter comparable to or smaller than the center wavelength of terahertz radiation. *Opt. Lett*. **27**, 1067, DOI: 10.1364/OL.27.001067 (2002)
16. Wu, Q. & Zhang, X. Free-space electro-optic sampling of terahertz beams. *Appl. Phys. Lett.* **67**, 3523–3525, DOI: 10.1063/1.114909 (1995)
17. Planken, P. C. M. *et al*. Measurement and calculation of the orientation dependence of terahertz pulse detection in ZnTe. *J. Opt. Soc. Am. B.* **18**, 313, DOI: 10.1364/JOSAB.18.000313 (2001)
18. Withayachumnankul, W. *et al.* Uncertainty in terahertz time-domain spectroscopy measurement. *J. Opt. Soc. Am. B.* **25**, 1059, DOI: 10.1364/JOSAB.25.001059 (2008)
19. Rehn, A. *et al.* Periodic sampling errors in terahertz time-domain measurements. *Opt. Express* **25**, 6712 DOI: 10.1364/OE.25.006712 (2017)
20. Lin, S., Yu, S. & Talbayev, D. Measurement of Quadratic Terahertz Optical Nonlinearities Using Second-Harmonic Lock-in Detection. *Phys. Rev. Appl.* **10**, 044007, DOI: 10.1103/PhysRevApplied.10.044007 (2018)
21. Xin, X. *et al.* Terahertz absorption spectrum of para and ortho water vapors at different humidities at room temperature. *J. Appl. Phys.* **100**, 094905, DOI: 10.1063/1.2357412 (2006)
22. Fattinger, C., Grischkowsky, D. & Exter, Martin van. Terahertz time-domain spectroscopy of water vapor. *Opt. Lett*, **14**, 20, 1128-1130, DOI: 10.1364/OL.14.001128 (1989)
23. Clerici, M. *et al.* Wavelength Scaling of Terahertz Generation by Gas Ionization. *Phys. Rev. Lett.* **110**, 253901, DOI: 10.1103/PhysRevLett.110.253901 (2013)
24. Van Der Valk, N., Wenckebach, T. & Planken, P. Full mathematical description of electro-optic detection in optically isotropic crystals. *J. Opt. Soc. Am. B.* **21**, DOI: 10.1364/JOSAB.21.000622 (2004)
25. Skellam, J. G. The Frequency Distribution of the Difference Between Two Poisson Variates Belonging to Different Populations. *J. Royal Stat. Soc.* **109**, 296–296, DOI: 10.2307/2981372 (1946)
26. Gan, H. L. & Kolaczyk, E. D. Approximation of the difference of two Poisson-like counts with Skellam. DOI: 10.48550/arXiv.1708.04018 (2018)

27. Bouchard, F. *et al*. Quantum Communication with Ultrafast Time-Bin Qubits. *PRX Quantum.* **3**, 010332, DOI: 10.1103/PRXQuantum.3.010332 (2022)

Acknowledgements

M.C. and A.C.D. acknowledge the support from the UK Research and Innovation (UKRI) and the UK Engineering and Physical Sciences Research Council (EPSRC) (Fellowship "In-Tempo" EP/S001573/1). M.C. and L. H. acknowledge the support from the Defence Science and Technology Laboratory (DSTL), DSTLX-1000144632. M.C., S.Y., L.C. acknowledge the support from Innovate UK, Application Number PN 10001572. D.F. acknowledges financial support from the Royal Academy of Engineering Chairs in Emerging Technology Scheme and from the UK Engineering and Physical Sciences Research Council (grants EP/M01326X/1 and EP/R030081/1).

Author contributions statement

T.S., A.C.D., L.C. and M.C. designed the experiment. T.S. performed the measurements with contributions from A.C.D and M.C. T.S., A.C.D., L.H., S.Y analyzed the data and interpreted the results. J.M.R.W., D.F., L.C., M.P., M.C. provided technical support to the experiment, data analysis, and interpretation of the results. T.S., A.C.D., S.Y. and M.C. drafted the manuscript. M.C. supervised the research activity. All authors reviewed the manuscript.

Additional information

All data underpinning this publication are available at the following address DOI: 10.5525/gla.researchdata.1330. The authors declare no competing interests.